ERDA/JPL/954344-76/4

WEB-DENDRITIC RIBBON GROWTH

Quarterly Report, October 1, 1976—December 15, 1976

R. B. Hilborn, Jr.
J. W. Faust, Jr.

December 28, 1976

Work Performed Under Contract No. NAS-7-100-954344

College of Engineering
South Carolina University
Columbia, South Carolina

ENERGY RESEARCH AND DEVELOPMENT ADMINISTRATION
Division of Solar Energy

DISCLAIMER

Printed in the United States of America
USERDA Technical Information Center, Oak Ridge, Tennessee

ERDA/JPL/954344-76/4
Distribution Category UC-63

Web-Dendritic Ribbon Growth

USC Solar Report No. Q-4

Quarterly Report for Period 10-1-76 to 12-15-76

Authors: R. B. Hilborn, Jr. and J. W. Faust, Jr.

Date of Publication: 12-28-76

JPL Contract No. 954344

Contractor: University of South Carolina
College of Engineering
Columbia, S. C. 29208

This work was performed for the Jet Propulsion Laboratory, California Institute of Technology, under NASA Contract NAS7-100 for the U.S. Energy Research and Development Administration, Division of Solar Energy.

The JPL Low-cost Silicon Solar Array Project is funded by ERDA and forms part of the ERDA Photovoltaic Conversion Program to initiate a major effort toward the development of low-cost solar arrays.

TABLE OF CONTENTS

SUBJECT	PAGE
Technical Content Statement	1
Abstract	1
Man-hours and Cost Totals	1
Summary of Results	1
Review by Tasks	2
Interpretation of Results	26
Tentative Conclusions	27
Projection of Next Quarter's Activity	27
Summary of Characterization Data	28
Program Plan	Attachment

Technical Content Statement

This report contains information prepared by the University of South Carolina under JPL subcontract. Its' content is not necessarily endorsed by the Jet Propulsion Laboratory, California Institute of Technology, National Aeronautics and Space Administration, or the U.S. Energy Research and Development Administration, Division of Solar Energy.

Abstract

This is a report of the fifth quarter's work on the web-dendritic ribbon growth at the University of South Carolina. A brief description of the work initiated and carried out during this period to meet the program goals is given along with a copy of the Program Plan covering the entire period of the contract.

Man-Hours and Cost Totals

Previous		Current Quarter*		Cumulative*	
Man-hours	Cost	Man-hours	Cost	Man-hours	Cost
13,356	$176,303	3248	$44,780	16,604	$221,083

*Figures include cost estimates for entire month of December, 1976.

Summary of Results

The web growth portion of this program was spent in the design, installation and testing of a new furnace geometry for the growth of dendritic web ribbon. The new installation was completed and the testing 90% accomplished. Results of the testing to determine the effect of the relative position of the r.f. coil with respect to the susceptor on the thermal profile in the melt are included in this report.

The one-dimensional thermal model has been used to determine the relationship between growth rate, web thickness, and mensicus height for stable growth. The results of this analysis are included in this report.

An analysis was completed of the thermal radiation from the meniscus including the effect of the curvature of the meniscus with the results indicating that inclusion of the curvature leads to approximately a 10% increase in the radiation loss.

Review by Tasks

T.E. 1.2: Web Growth

Due to the poor results from our initial furnace configuration reflected in our inability to reproducibly grow two dendrite web ribbon, a completely new furnace geometry was fabricated and installed. The new design was based on suggestions from the Westinghouse group who are also working on dendritic web silicon on another JPL contract and on suggestions from our own group working on the analysis of web growth. The new configuration shown in Figure 1 reflects changes in the design of: the r.f. coil, the top and bottom heat shields and the pedestal mount.

The heat shielding at the top consists of two heat shields, an upper thin (.06") shield and a lower thick (.25") shield. Each of these shields contains a dogbone slot, through which the ribbon is pulled, having the following dimensions:

Straight portion

Length = 1.3"
Width = 0.375"

End portions

Length perpendicular to slot length = 7/8"
Length parallel to slot length = 5/8"

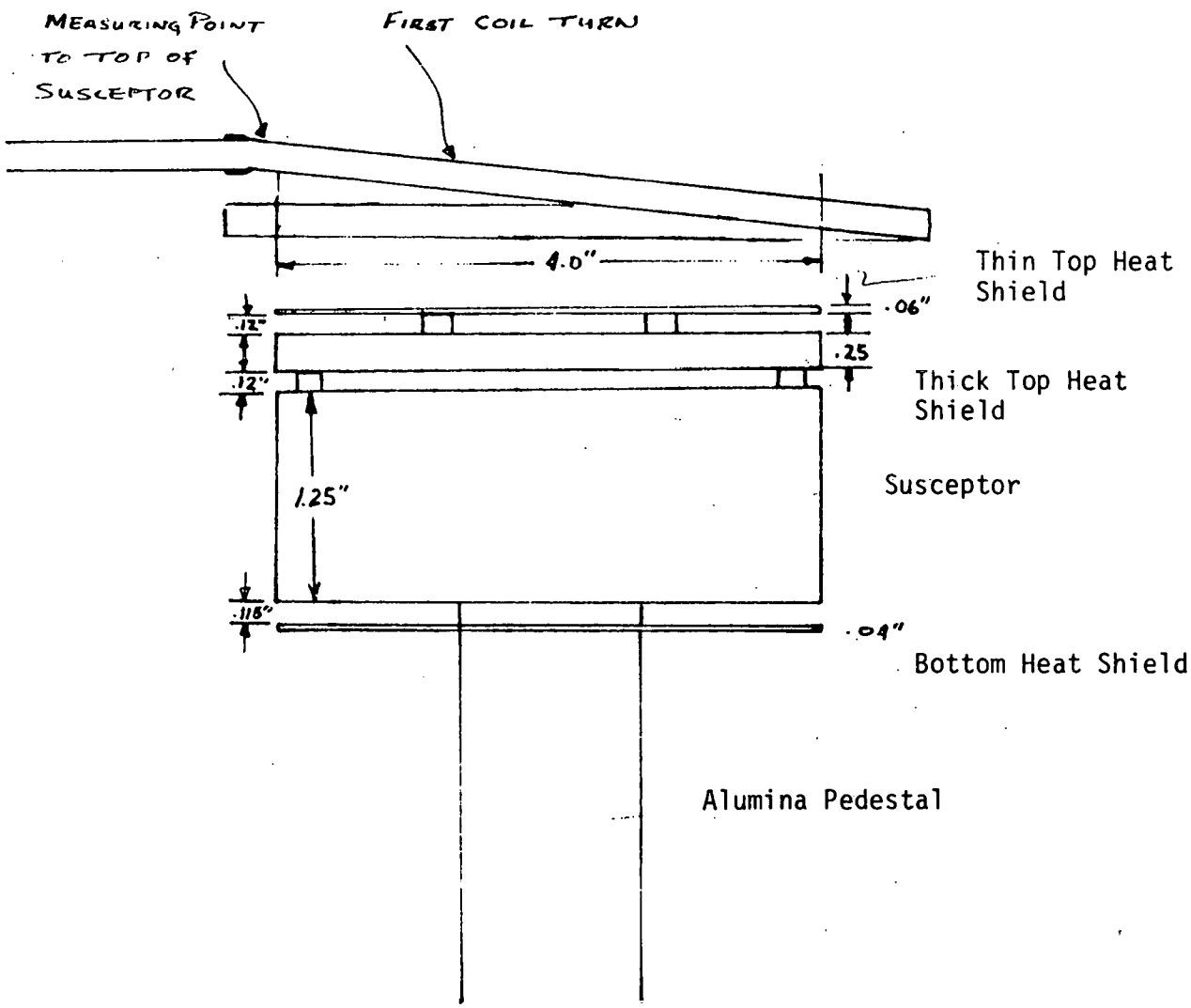

Figure 1: New Furnace Geometry

These shields were fabricated from 4" diameter molybdenum sheet.

The bottom heat shield consists of a 4" diameter thin (.025") sheet of alumina with one radial slot to prevent cracking due to thermal shock.

The pedestal consists of three concentric alumina tubes. The outside diameter of the outer tube is 2 1/4". The outer tube serves to support the 4" diameter bottom alumina heat shield. The middle tube supports the molybdenum susceptor and the inner tube is used to support molybdenum heat shields within the support tube to prevent thermal losses down the otherwise hollow pedestal.

The r.f. coil design was changed to a shorter length while containing the same number of total turns as on the previous coil. This was done to concentrate the power input to the region of the susceptor. The previous coil design was so long that when positioned correctly to melt the charge in the susceptor, too much coupling occurred with the top heat shields. This caused the top shields to be at such a high temperature that the web would invariably fall out from between the two edge dendrites when the ribbon was pulled up through the slots in the shields.

The entire quarter has been spent in the design, installation, and testing of this new furnace geometry. The testing consisted of measuring the thermal profiles with thermocouples in the melt as a function of r.f. coil position relative to the susceptor. These results are shown in Figures 2 through 9.

In addition to the previously mentioned changes in furnace design, a modification to the take-up reel was made enabling us to pull the ribbon from the melt at a slower rate than previously. Our pull rates now range from 1 to 4 cms/min. This was done as it was felt that part of our difficulty in pulling the web ribbon through the slots in the top heat shields may have been caused by not pulling sufficiently slowly initially to allow the button to lose some of its thermal energy by radiation prior to being pulled through the slots.

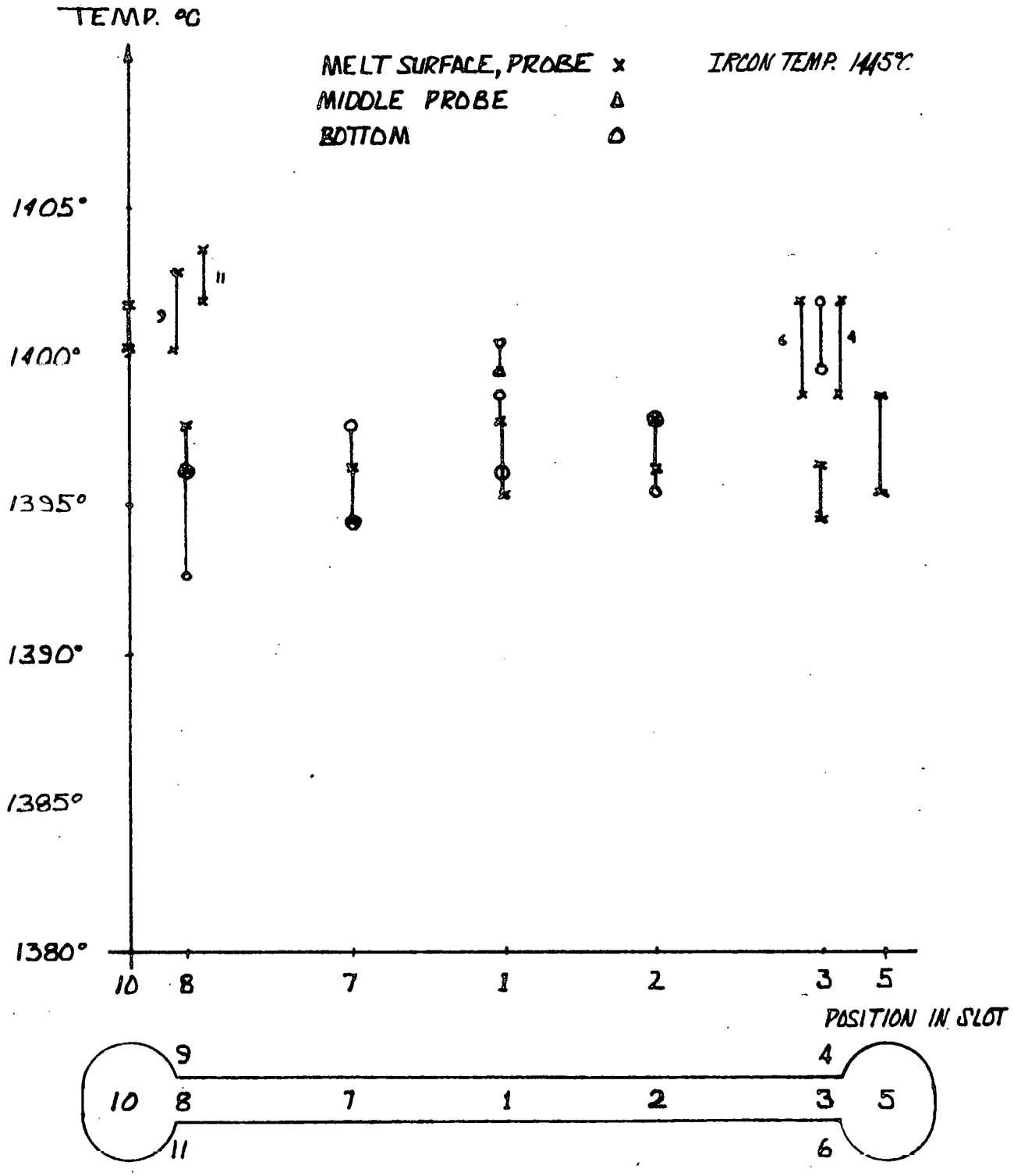

Figure 2: Thermal Profiles in Melt for Various Coil Positions

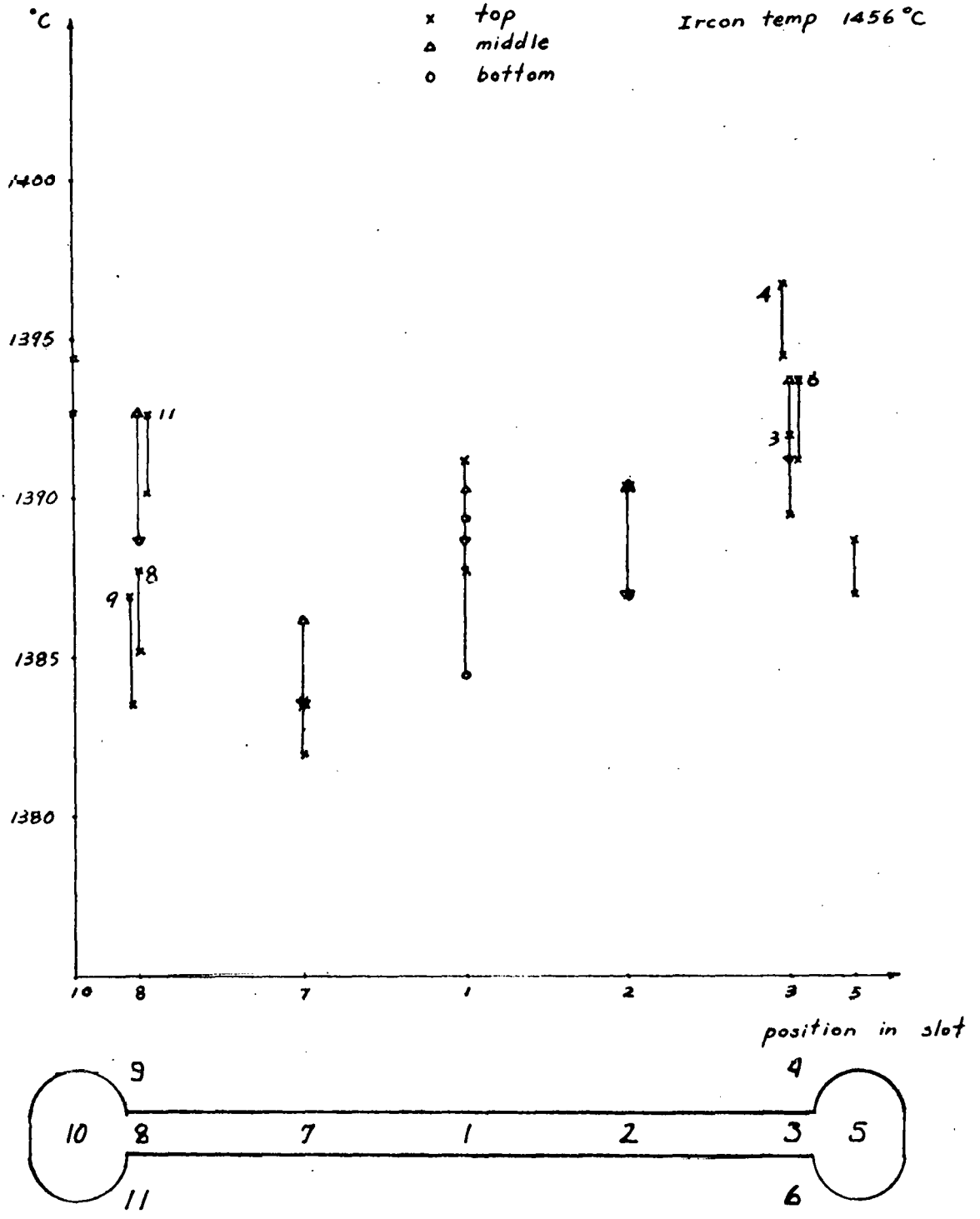

Figure 3: Thermal Profiles in Melt for Various Coil Positions

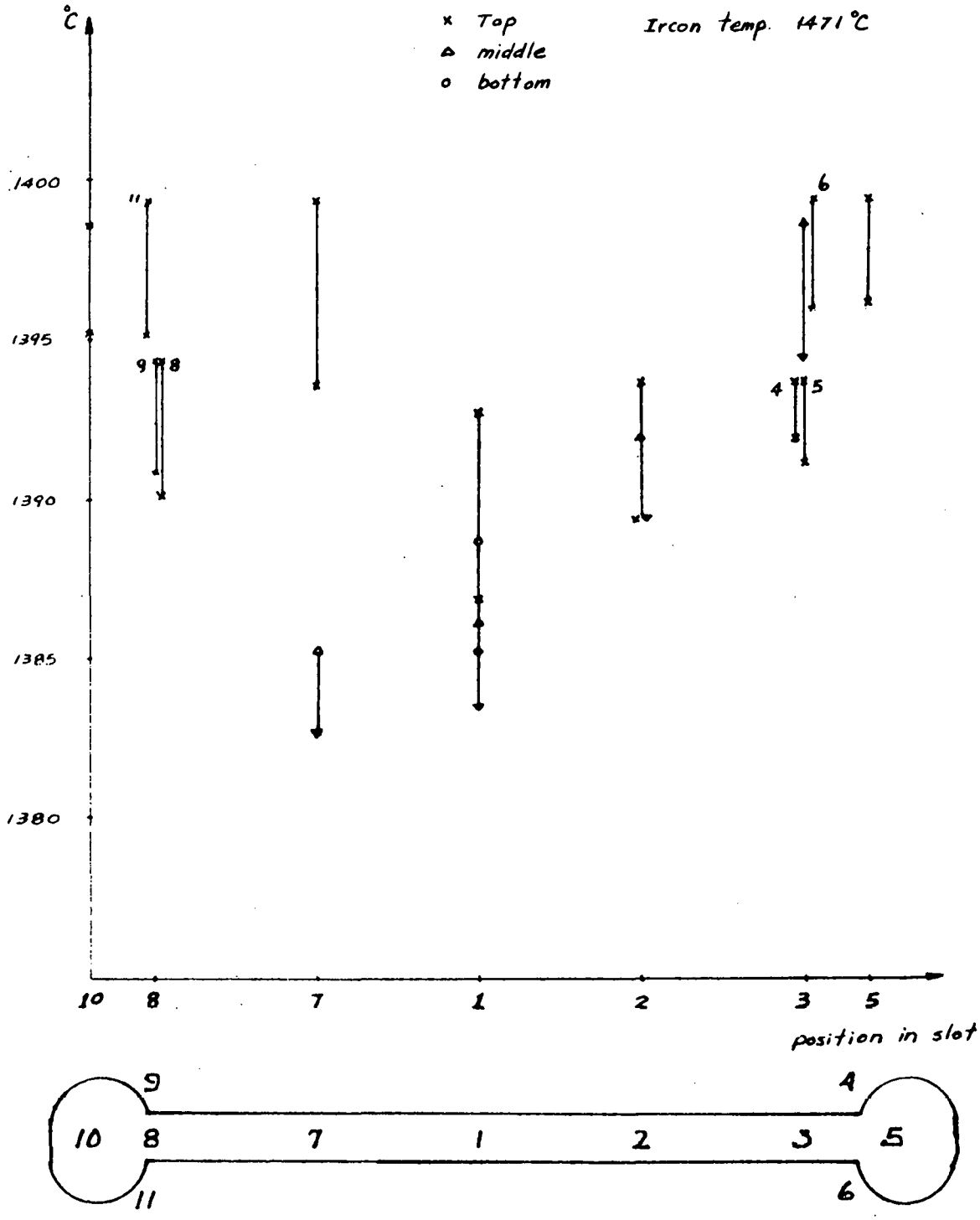

Figure 4: Thermal Profiles in Melt for Various Coil Positions

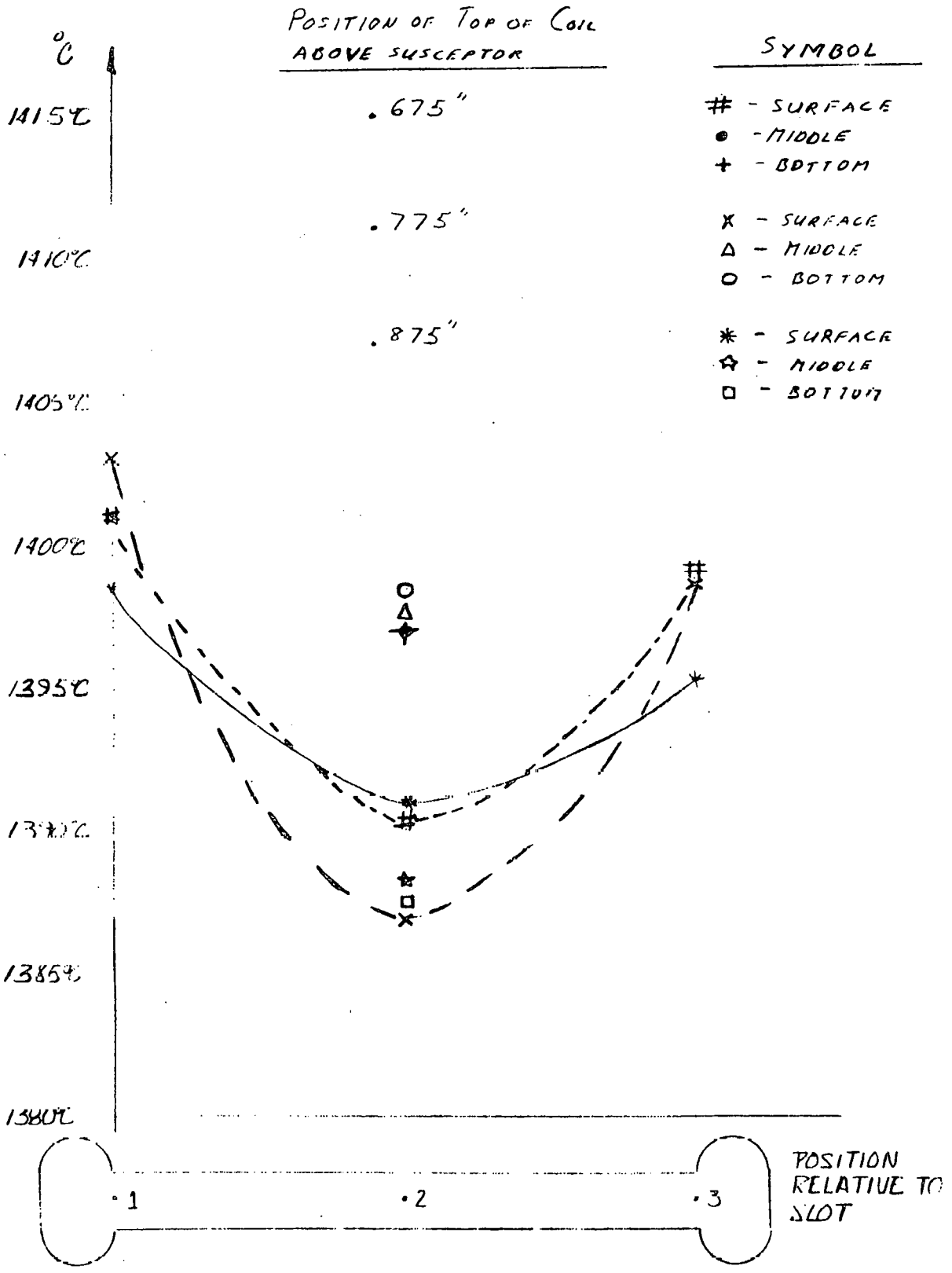

SET UP: .06"x4" TOP SHIELD. MOLY.
1.25"x4" SUSCEPTOR. MOLY.
.025"x4" BOTTOM SHIELD MOLY.
CERAMIC PEDESTAL

Figure 5: Thermal Profiles in Melt for Various Coil Positions

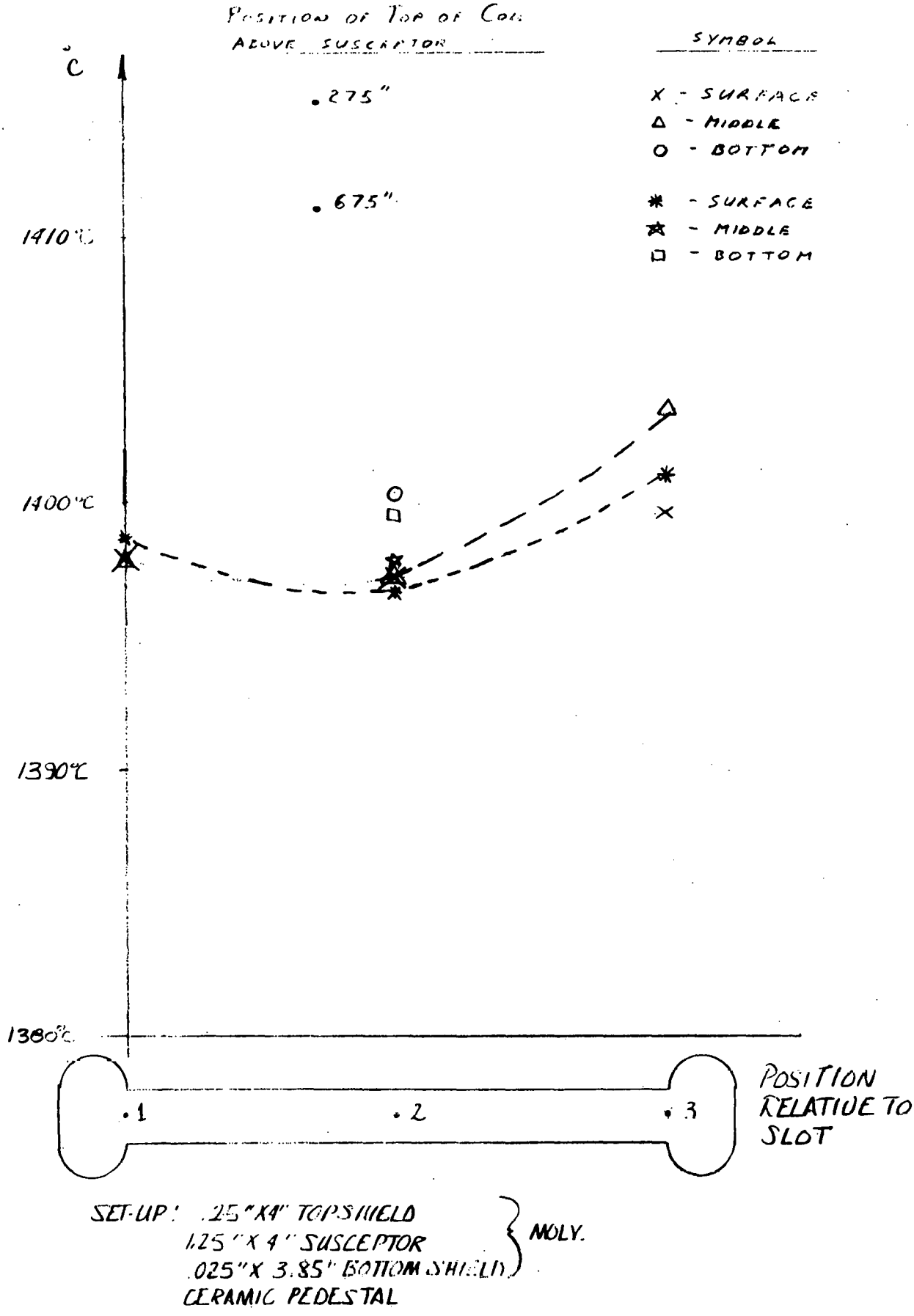

Figure 6: Thermal Profiles in Melt for Various Coil Positions

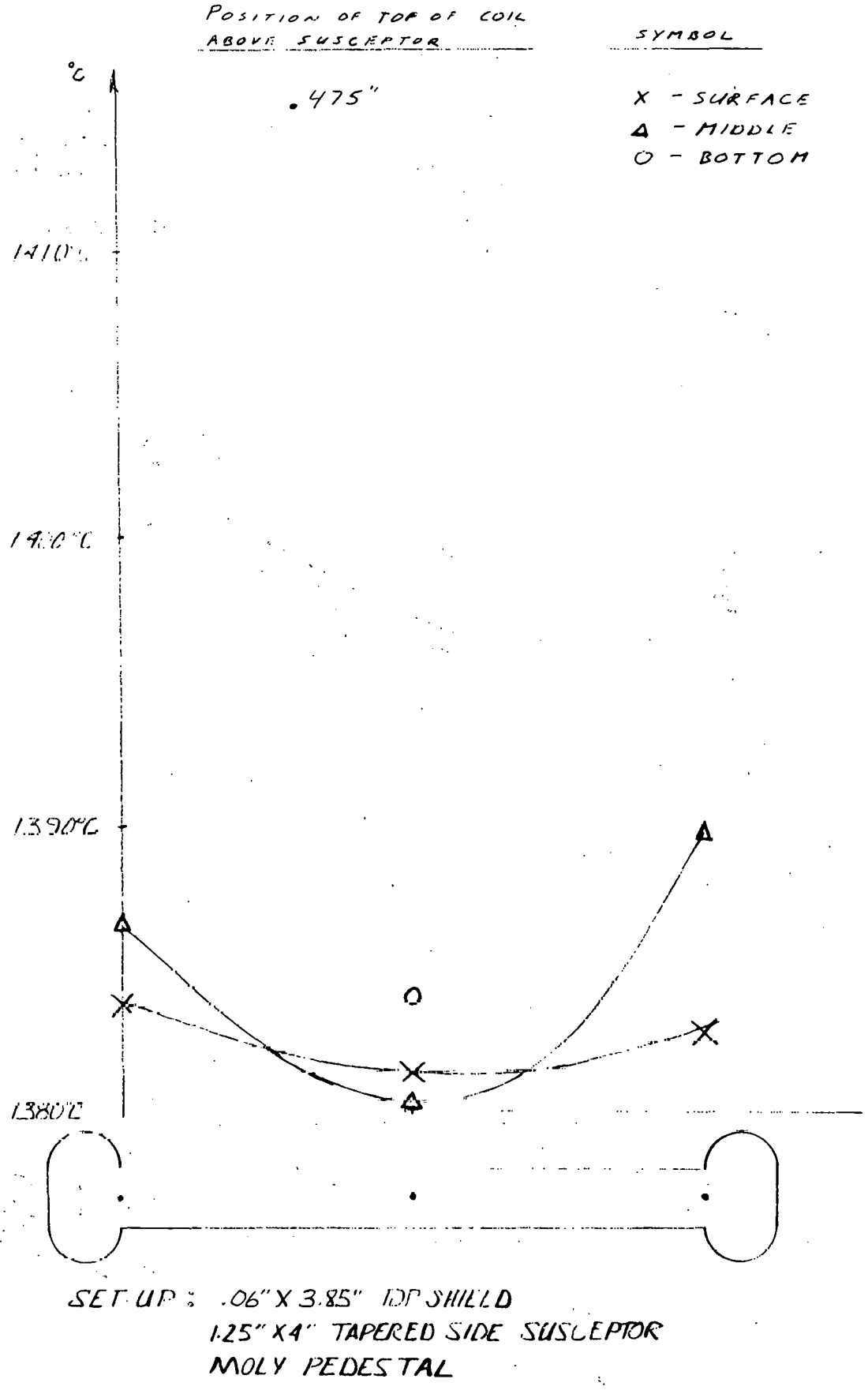

Figure 7: Thermal Profile in Melt for Various Coil Positions

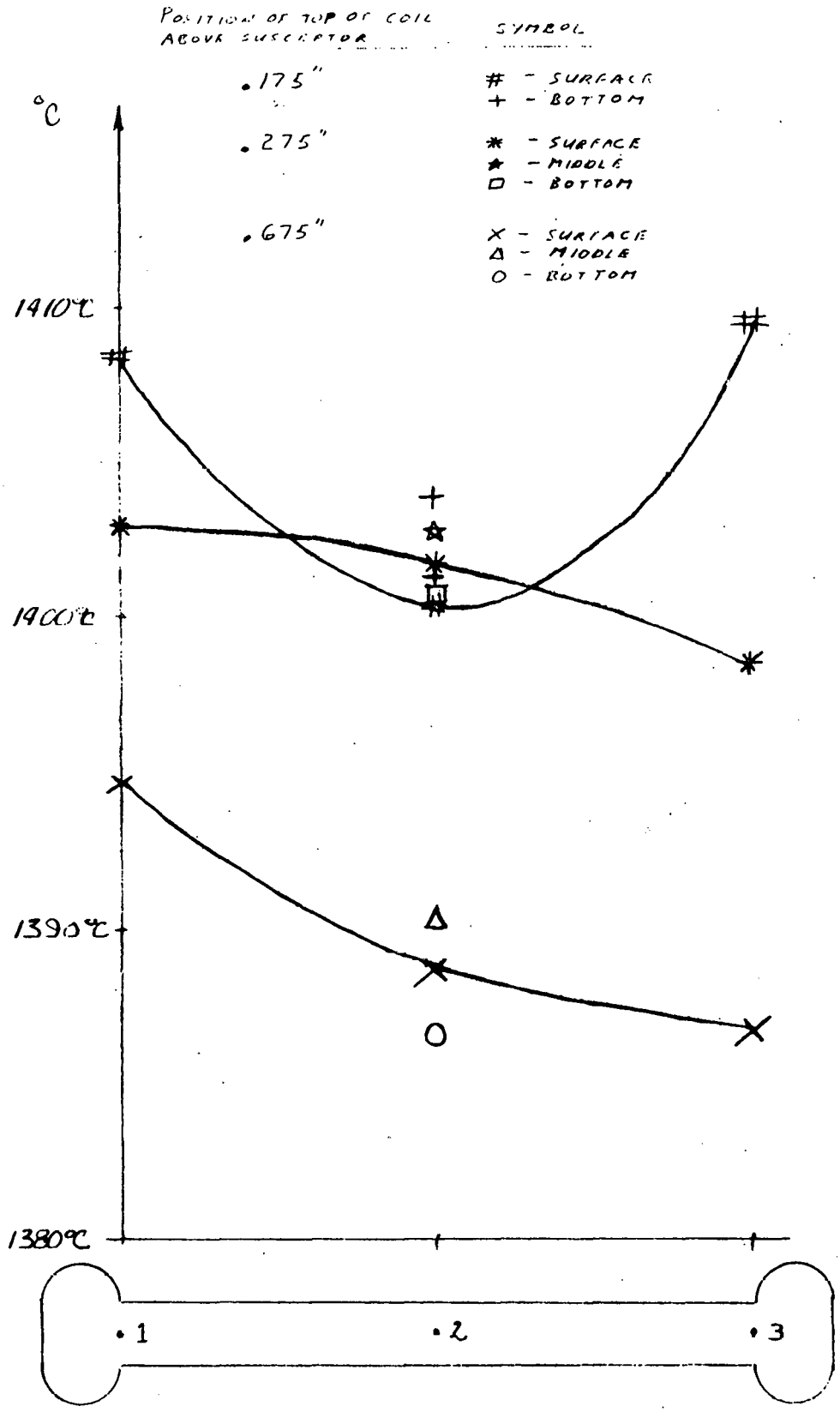

SET-UP : .06" \ 4" TOP SHIELD
1.25" X 4" SUSCEPTOR } MOLY
.025" X 3.85" BOTTOM SHIELD
CERAMIC PEDESTAL

Figure 8: Thermal Profiles in Melt for Various Coil Positions

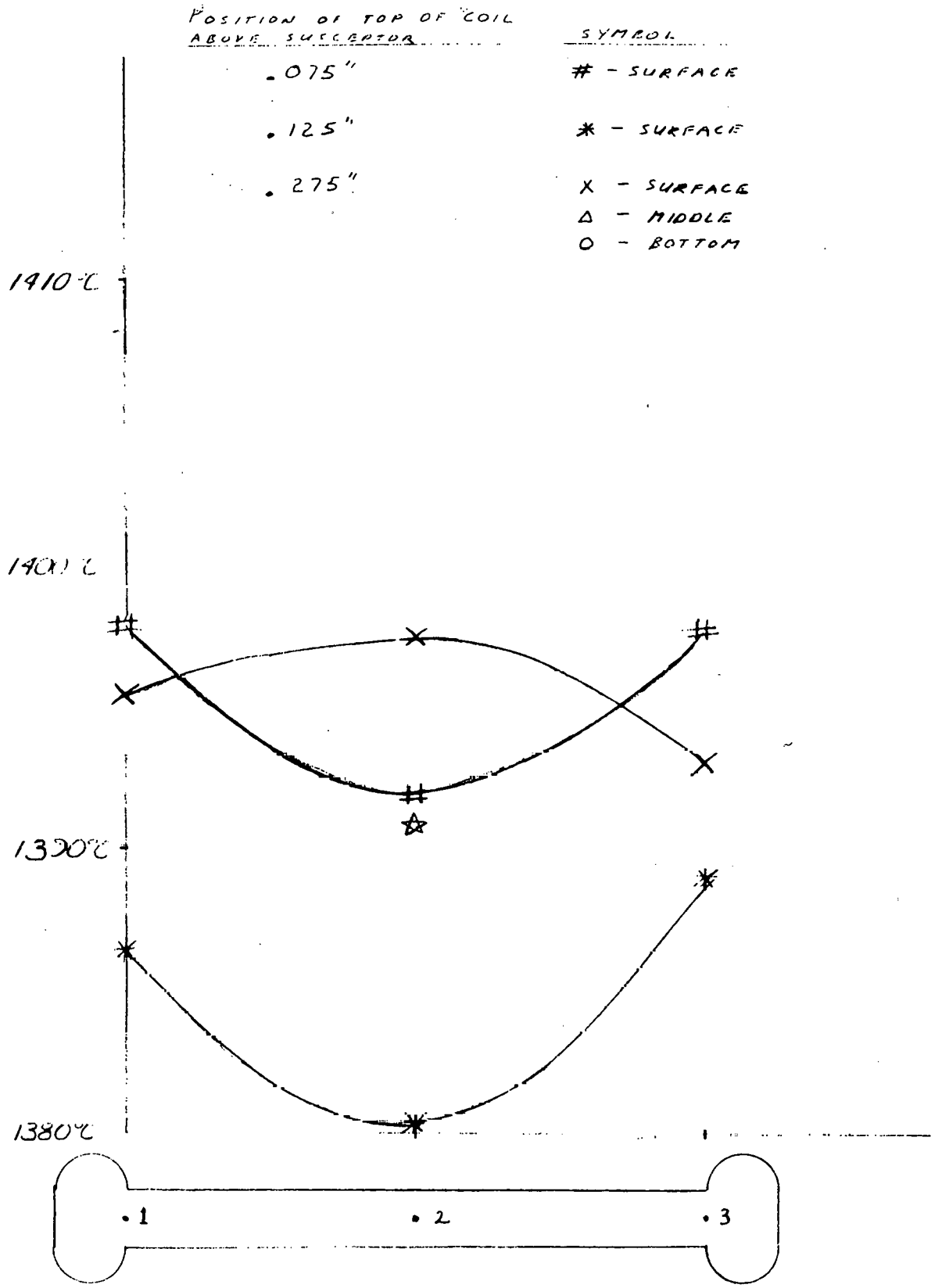

SET UP : .06"X4" TOP SHIELD
1.25"X4" SUSCEPTOR
.025"X 3.85" BOTTOM SHIELD
CERAMIC PEDESTAL

Figure 9: Thermal Profile in Melt for Various Coil Positions

Due to a breakdown of our r.f. generator during the last 3 weeks of this report period, insufficient data is available to evaluate the results of our furnace geometry changes on our ability to reproducible grow two-dendrite web ribbon.

T. E. 1.3: Web Growth Analysis

T. E. 1.3.1: Thermal Modeling of Web Growth

The one-dimensional thermal model [1] has been used to determine the relationship between growth rate, web thickness, and meniscus height for stable growth. Details of the mathematical model and numerical technique are given by Harrill [2]. Thermal radiation heat exchange between the web, melt surface, and thermal shield was included in the model. The meniscus surface and a portion of the web exchange thermal radiation with the horizontal melt surface and the underside of the thermal shield. The region of the web above the thermal shield exchanges radiation with the upper surface of the thermal shield.

It was assumed in the calculations that the distance between the surface of the melt and the thermal shield is 1.4 cm. Since the melt temperature must be maintained slightly supercooled (2 °C - 5 °C) in order to obtain dendritic growth, the temperature of the melt entering the meniscus is also supercooled. The temperature assumed in the calculations is 1407 °C. When the melt reaches the liquid-solid interface its' temperature increases to approximately the melting temperature of 1412 °C. The increase in the temperature of the melt as it flows up the meniscus is due to the latent heat of fusion at the liquid-solid interface.

Results of meniscus geometry studies by Hilborn and Faust [1] have shown that the meniscus height is determined by the meniscus joining angle.

The joining angle is defined as the angle between the surface of the melt and the vertical at the liquid-solid interface. Large joining angles result in lower meniscus heights. Joining angle has been chosen as a parameter rather than meniscus height since it is expected that stable growth may be limited to a small range of joining angles. For example, Mika and Uelhoff [3] predicted constant diameter Czochralski growth for a zero joining angle. Swartz, Surek, and Chalmers [4] predicted a small but positive joining angle of approximately 11° for the EFG technique based on experimental data from horizontally grown silicon wafers. The appropriate joining angle for web-dendritic growth has not been determined and will be studied further.

Figure 10 shows the predicted pull rate as a function of joining angle for web thicknesses of 0.10 mm, 0.15 mm, and 0.20 mm. These values are predicted for a thermal shield temperature of 1300 °C. It is seen that the pull rate decreases as web thickness increases for constant joining angle. In addition, the pull rate decreases as joining angle increases. The pull rates are seen to be in the region from approximately 2 - 4 cm/min which is approximately within the range of the experimental pull rates.

The decrease in the pull rate with increasing joining angle is caused by a decrease in the meniscus height. At small joining angles the meniscus height is high, which provides considerable radiation area for radiating heat. A significant quantity of the latent heat of fusion released at the liquid-solid interface is conducted into the liquid meniscus and radiated to the environment. As the joining angle increases meniscus height decreases and less surface area is available for radiating heat causing the pull rate to decrease.

Figure 11 shows the melt temperature in the meniscus as a function of elevation above the melt surface for a joining angle of zero degrees and web

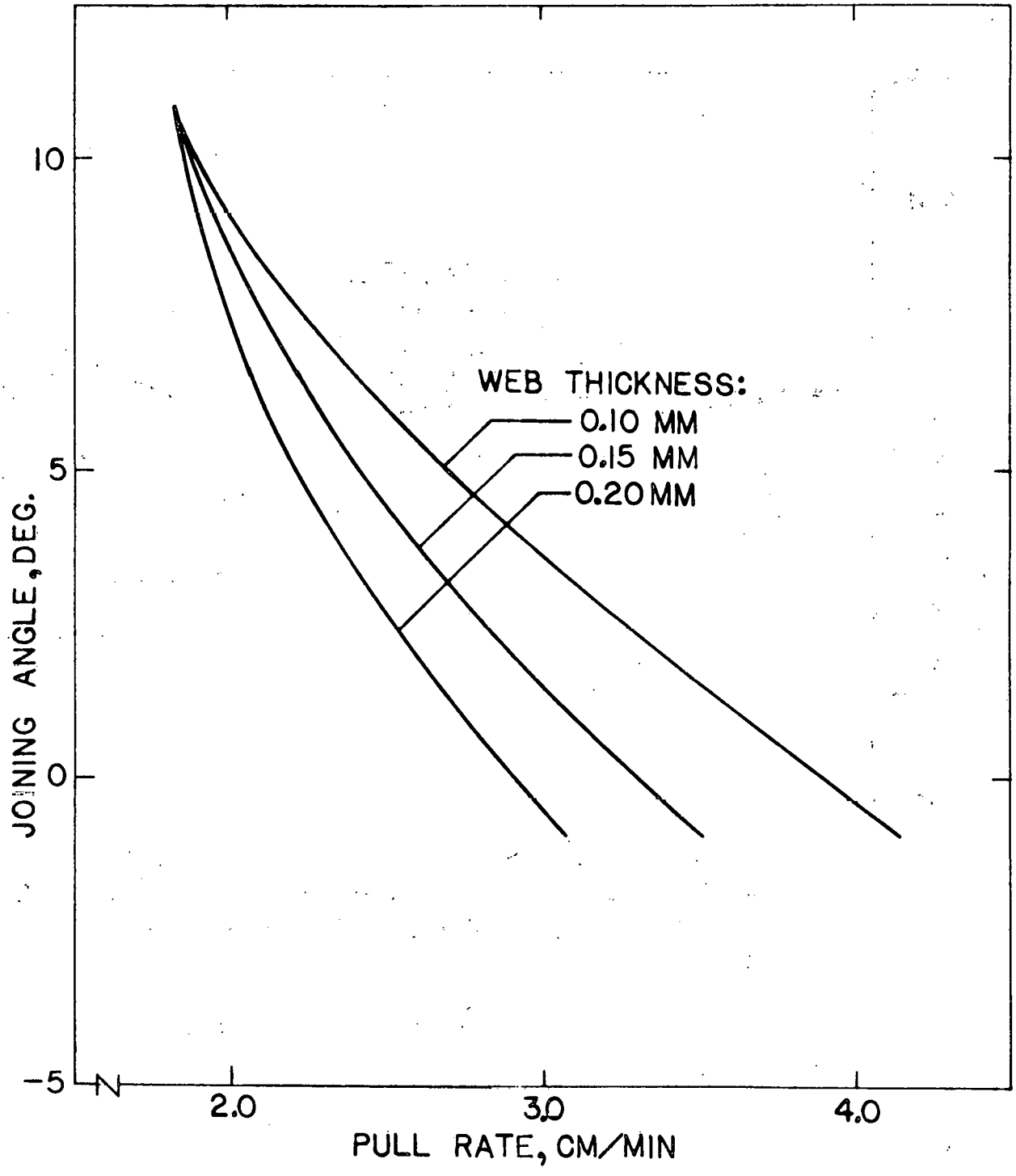

Figure 10: Joining Angle as a Function of Pull Rate for Constant Web Thickness. Thermal Shield Temperature Equal 1300 °F and Distance Between Melt and Thermal Shield is 1.4 cm.

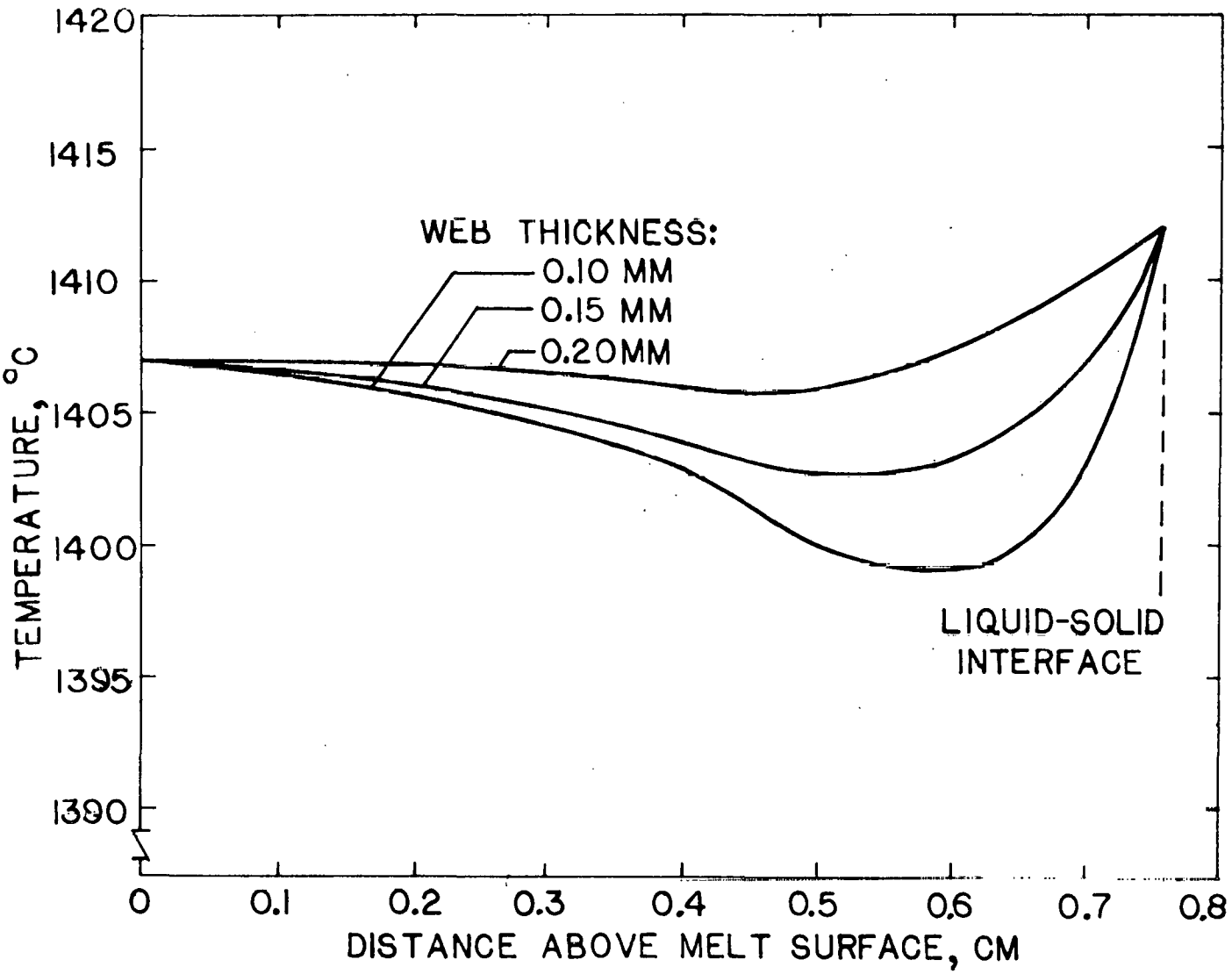

Figure 11: Temperature of Melt in Meniscus for Zero Degree Joining Angle.

thicknesses of 0.10 mm, 0.15 mm, and 0.20 mm. The liquid-solid interface is on the right side of the graph where all three curves reach 1412 °C. It is seen that all three curves have a negative temperature gradient at the liquid-surface and, therefore, heat is conducted from the interface to the melt. Figure 12 shows the same three curves for a joining angle of 10 degrees. The temperature gradient is also negative but much less so than in Figure 11.

Pull rate is affected by both the temperature of the thermal shield and also by the distance between the thermal shield and the melt surface. Figure 13 shows the effect of thermal shield temperature on the pull rate. These results are plotted for a joining angle of zero degrees. As expected, decreasing the thermal shield temperature results in an increase in pull rate. For example, decreasing thermal shield temperature from 1300 °C to 1100 °C increases the pull rate from 3.9 cm/min to 5.7 cm/min for a web thickness of 0.10 mm.

The effect of the distance between the melt surface and the thermal shield is currently being investigated but it is obvious that decreasing this distance results in an increase in pull rate. How significantly this distance affects pull rate is yet to be determined.

It must be pointed out that the temperature of the melt in the crucible is affected by the thermal shield temperature. Consequently, there may be some lower limit on the thermal shield temperature at which web growth is possible. At the present time, it does appear that the effect of thermal shield temperature on growth is well defined. Further study is currently being performed in an attempt to understand this relationship.

Since the distance between the melt and thermal shield also affects the temperature of the melt in the crucible, it may not be possible to choose the distance to obtain maximum growth rate. Further study is needed here also.

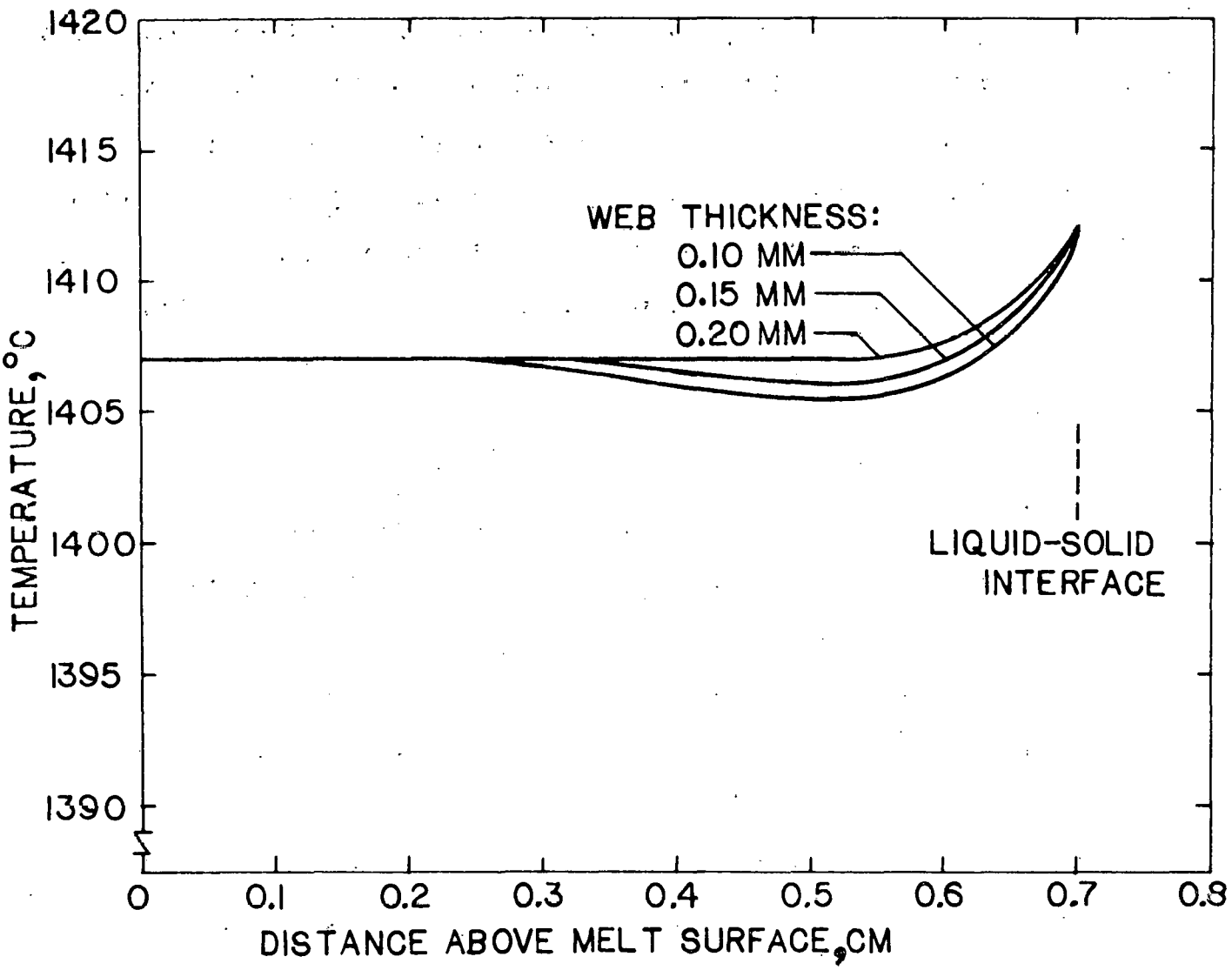

Figure 12: Temperature of Melt in Meniscus for 10 Degree Joining Angle.

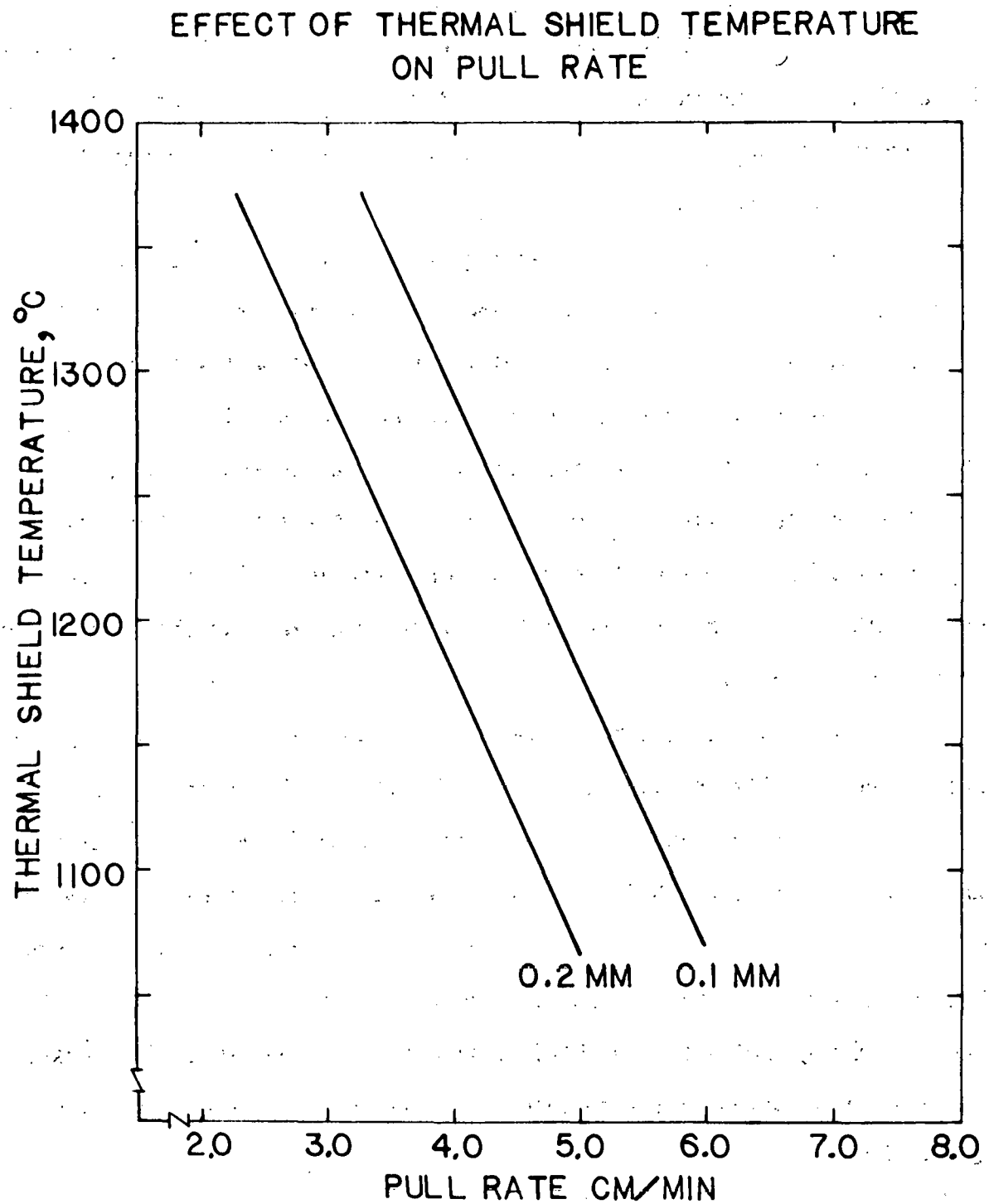

Figure 13: Variation of Pull Rate with Thermal Shield Temperature at Zero Degrees Joining Angle and 1.4 cm Spacing Between Melt and Thermal Shield.

T. E. 1.3.2: Thermal Radiation From Meniscus

Thermal radiation emitted from the surface in the region of the meniscus experiences multiple reflections, absorptions, and re-emissions before escaping to the surroundings. As a consequence, the radiation losses are smaller in this region than for the horizontal melt surface. In the analysis described in Section 1.3.1 the curvature effects of radiation losses were neglected, thus the purpose of the present investigation was to determine the importance of the curvature effect on heat losses.

The radiant heat flux leaving the surface (radiosity) in the meniscus region was determined also. Due to the multiple reflections in the meniscus, the radiosity is greater than that of the horizontal melt surface. As a consequence of the greater radiosity, the meniscus region appears bright to an observer. The "bright ring" observed at the meniscus during Czochralski growth results from the curvature effect. The radiosity characteristics of the meniscus is of importance when using radiation measurement techniques for the control of the web growth. A radiometer detects the radiant flux leaving the surface or radiosity of the surface.

The analysis was performed by dividing the surface into approximately one hundred parallel strips as shown in Figure 14. The surface was assumed gray, diffuse, and having a uniform temperature. Gebhart's method [5] of determining the absorption factors (Bij) for each of the surfaces was employed in the analysis. Since the web is wide compared to the meniscus height, the angle factors between each of the surfaces was determined assuming the strips were infinite. The meniscus geometries were obtained from Hilborn and Faust [1]. Results were obtained by solution on the computer and details of the study are given by Oster [6].

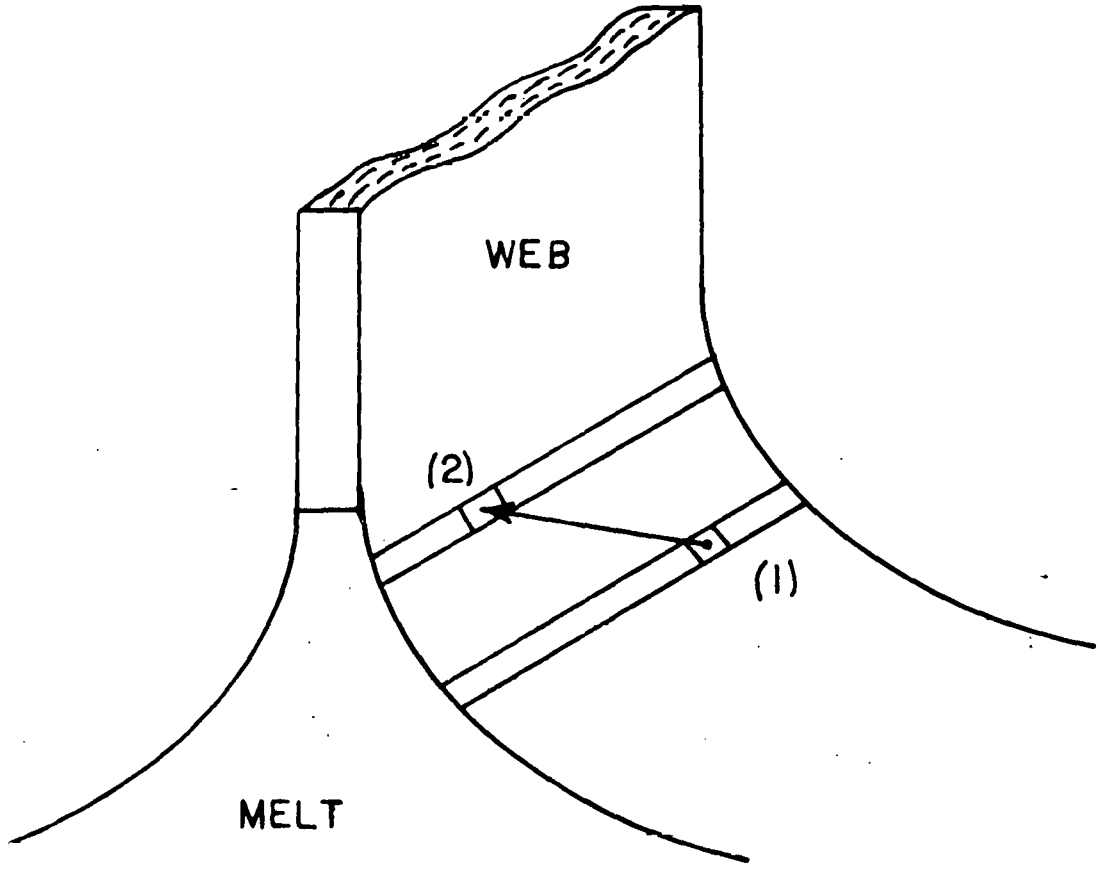

Figure 14: Radiation emitted from Area (1) of the Meniscus Irradiator Area(2) due to the Curvature of the Meniscus.

Figure 15 shows the heat loss as a function of distance from the melt surface. The dimensionless heat loss $Q/\varepsilon\sigma T^4$ is the ratio of heat loss per unit area in the meniscus to that of the horizontal melt surface. For ratios greater than unity, heat loss exceeds that of a horizontal surface and vice versa. The dimensionless height is the ratio of the position on the meniscus to height of the liquid-solid interface. The liquid-solid interface occurs at unity, however, the height of the liquid-solid interface depends upon contact angle.

At the melt surface, the dimensionless heat loss is unity and decreases with height reaching a minimum at the liquid-solid interface. The values for the three joining angles are similar except near the liquid-solid interface. The dip in the curve for the -10° joining angle results from "necking" in the meniscus for negative joining angles.

The radiosity of the meniscus is shown in Figure 16. The dimensionless radiosity $R/\varepsilon\sigma T^4$ is the ratio of the radiosity to that of a surface having no external radiation impinging on the surface. At points on the melt surface at large distances from the meniscus, the effect of curvature is small and the ratio is near unity. The radiosity increases by approximately 40% at the liquid-solid interface. The surface in this region should appear significantly brighter to an observer.

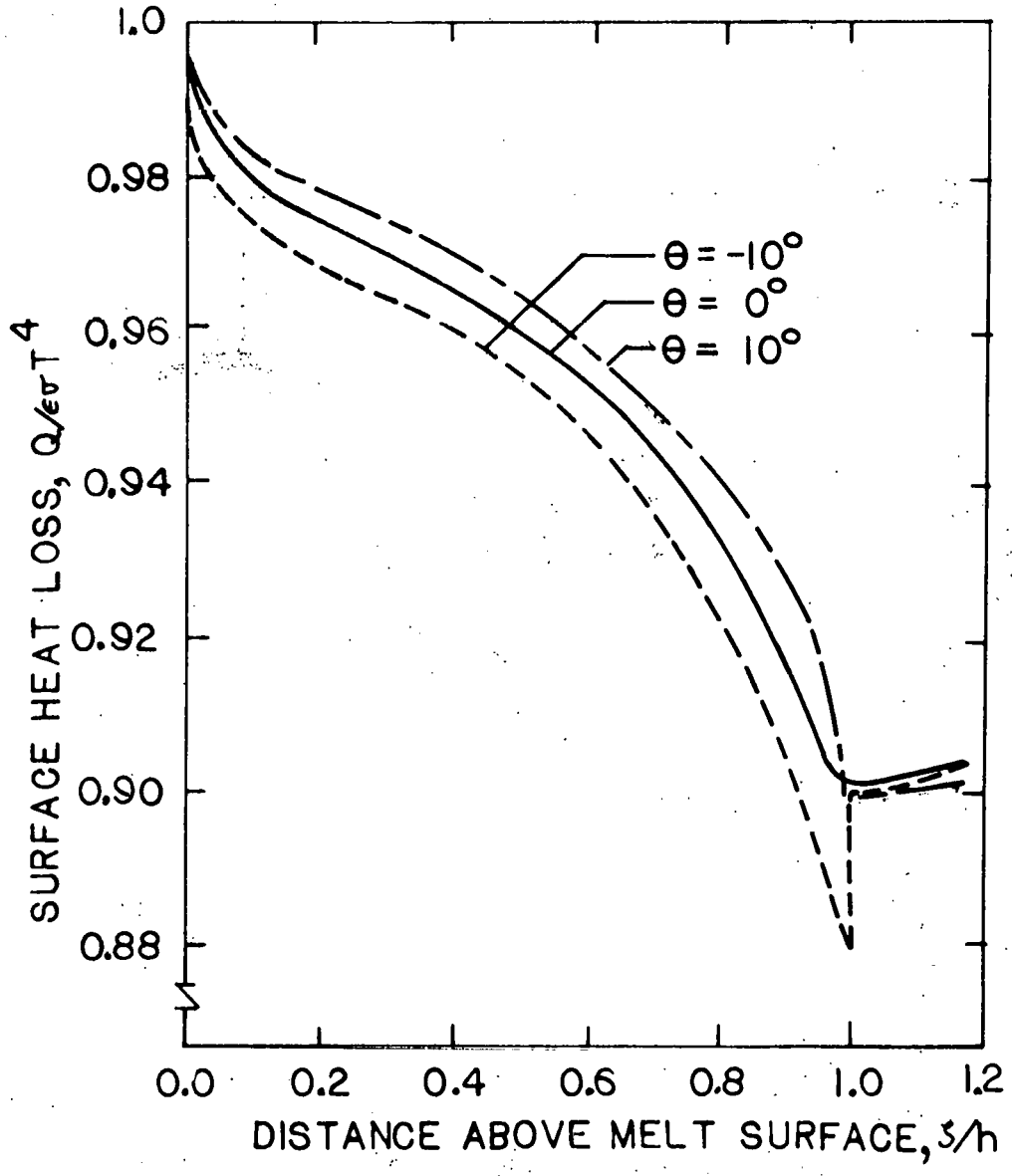

Figure 15: Ratio of Surface Heat Loss to that of Horizontal Melt Surface, $Q/\varepsilon\sigma T^4$, as a Function of the Ratio of Distance above Melt Surface to the Meniscus Height, ζ/h. Joining Angles are -10°, 0°, and 10°.

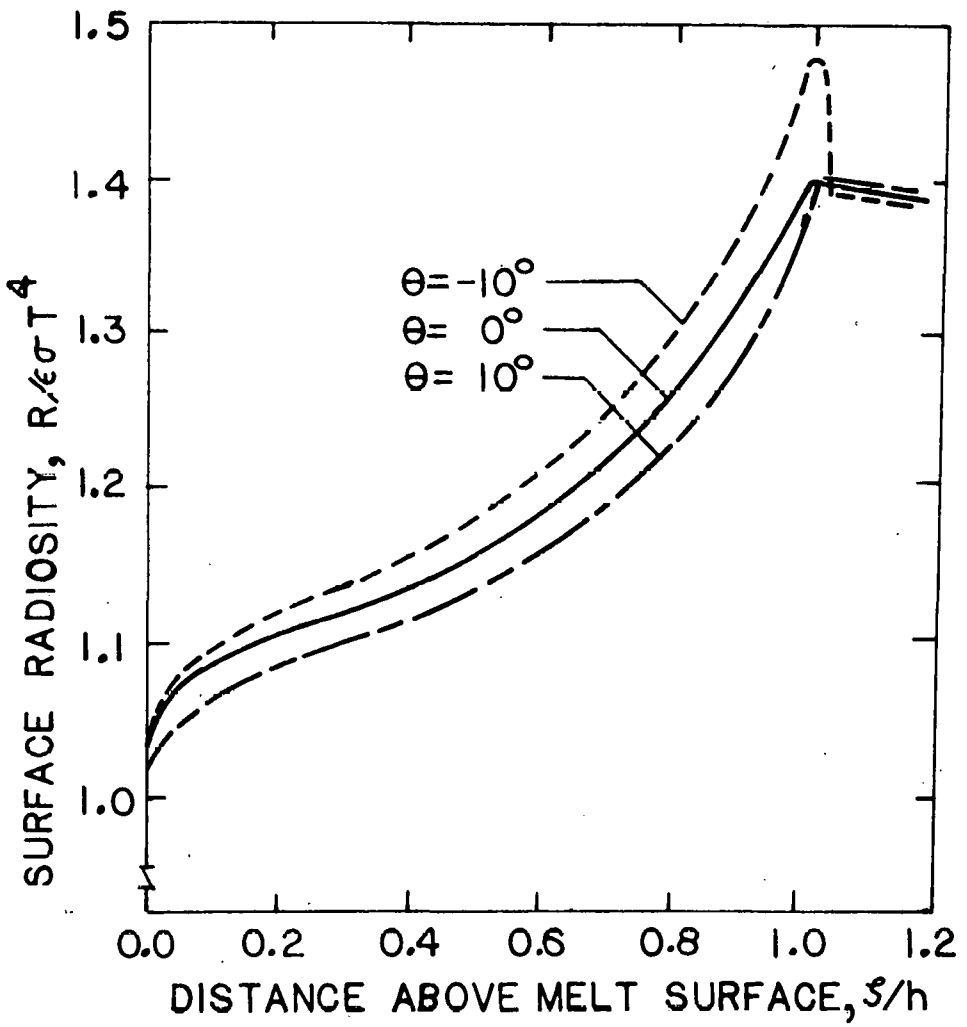

Figure 16: Ratio of Surface Radiosity to that of Horizontal Melt Surface, $R/\varepsilon\sigma T^4$, as a Function of the Ratio of Distance above the Melt Surface to the Meniscus Height, ζ/h. Joining Angles are -10°, 0°, and 10°.

BIBLIOGRAPHY

1. Hilborn, R.B., Jr., and J.W. Faust, Jr., Web-Dendritic Ribbon Growth, USC Solar Report No. A-1, Sept. 1976.

2. "Thermal Modeling of Web-Dendritic Ribbon Growth of Silicon", M.D. Harrill, M.S. Thesis, University of South Carolina, 1976.

3. Mika, K. and W. Uelhoff, "Shape and Stability of Menisci in Czochralski Growth and Comparison with Analytical Approximations", Journal of Crystal Growth, vol. 30, pp. 9-20, 1975.

4. Swartz, J.C., T. Surek, and B. Chalmers, "The EFG Process Applied to the Growth of Silicon Ribbons", Journal of Electronic Materials, vol. 4, no. 2, pp. 255-279, 1975.

5. Heat Transfer, B. Gebhart, McGraw-Hill, Inc,. New York, 1971.

6. "Thermal Radiation from Menisci for Web-Dendritic Growth of Silicon", J.R. Oster, M.S. Thesis, University of South Carolina, 1976.

T. E. 2.0. Characterization

No further characterization work was conducted in this quarter due to a lack of samples. The facilities for the characterization are in operational readiness.

Interpretation of Results and Applications to Program Goals

a. Web-Growth

The results of testing the new furnace geometry indicate that a considerable greater control and latitude over the thermal profile in the melt is possible with the new configuration than was possible with the old. The thermal profiles achieved appear adequate for the growth of dentritic web ribbon based on the information available on what thermal conditions are necessary for achieving this type of Si crystal growth. It appears that lateral thermal profiles on the melt surface can be achieved with either a positive or negative gradient from the center of the Si charge by proper location of the r.f. coil with respect to the susceptor. Furthermore, heat shield adjustments can be made to control the temperature gradients from top to bottom in the melt. Thus, once optimum conditions for button formation have been determined the vertical temperature gradient for ribbon growth can be varied by changes in the pull rate. It is thus felt that the new furnace configuration will now allow us enough control over the growth conditions to achieve two dendrite web ribbon growth.

b. Web Growth Analysis.

The results of this work to date would indicate that there is an inherent upper limit on the pull rate that can be achieved with dendritic-web crystal growth. Further work to include the effects of top shield temperature and height with respect to the melt surface are needed before this upper limit

can be established.

The results of including the curvature of the meniscus on the radiation losses from the meniscus indicates that the radiation loss is increased by something less than 10% by the curvature effect.

Tentative Conclusions and Recommendations

The new furnace geometry has been installed and testing nearly completed. It appears that the new configuration will be adequate for the growth of dendritic web ribbon.

The analytical work has indicated that an inherent upper limit will exist on the maximum pull rate achievable with dendritic web ribbon growth. The inclusion of the top heat shield temperature and height above the melt in the analytical model is necessary before this upper limit can be indentified.

Engineering Drawings and Sketches

The drawings and sketches generated during this report period are incorporated in the text of this report as Figures 1 through 16.

Projection of Activities for Succeeding Three Months

Testing of the new furnace geometry will be completed.

The optimum configuration for button formation and web growth will be selected and investigated thoroughly to achieve reproducible two-dendrite web ribbon.

The temperature and location of the top heat shield above the melt surface will be incorporated in the analytical model for web growth to determine the inherent upper limit of the pull rate to be expected for this type of crystal growth.

Characterization data will be generated based upon the availability of samples.

Summary of Characterization Data

No characterization data was generated during this report period.

PROGRAM PLAN

WEB-DENDRITIC RIBBON GROWTH

UNIVERSITY OF SOUTH CAROLINA

PERIOD: 1 OCTOBER 1975 - 1 MAY 1977

UPDATED 31 SEPTEMBER 1976

LEGEND:
- H - HILBORN
- F - FAUST
- R - RHODES
- A - RESEARCH ASSOCIATE
- G - GRADUATE ASSISTANT
- S - SECRETARY

(Figures in columns represent man hours committed)

1. Web Growth, Growth Analysis

1.1 Set up web furnace

1.1.1 Level, align, calibrate gas flow, measure physical/mechanical parameters

1.1.2 Instrument melt temperature sensors, run furnace and RF generator

1.1.3 Calibrate RF generator controls to melt temperature, no web pulling

1.2 Web growth, manual batch

1.2.1 Pull nominal web based on 1965 experience, establish measurements baseline. (Instrument melt level measurement), correlate with crystallization kinetics and seeding requirements

1.2.2 Vary pull rate, measure effects, correlate with crystallization kinetics and seeding requirements

1.2.3 Vary RF heat transfer rate, measure effects, correlate with crystallization kinetics and seeding requirements

1.2.4 Couple RF heat transfer rate and pull rate variations, measure effects, correlate with crystallization kinetics and seeding requirements

1.2.5 Final experimental design

1.2.6 Final manual variation of manipulated variables, correlation with crystallization kinetics and seeding requirements

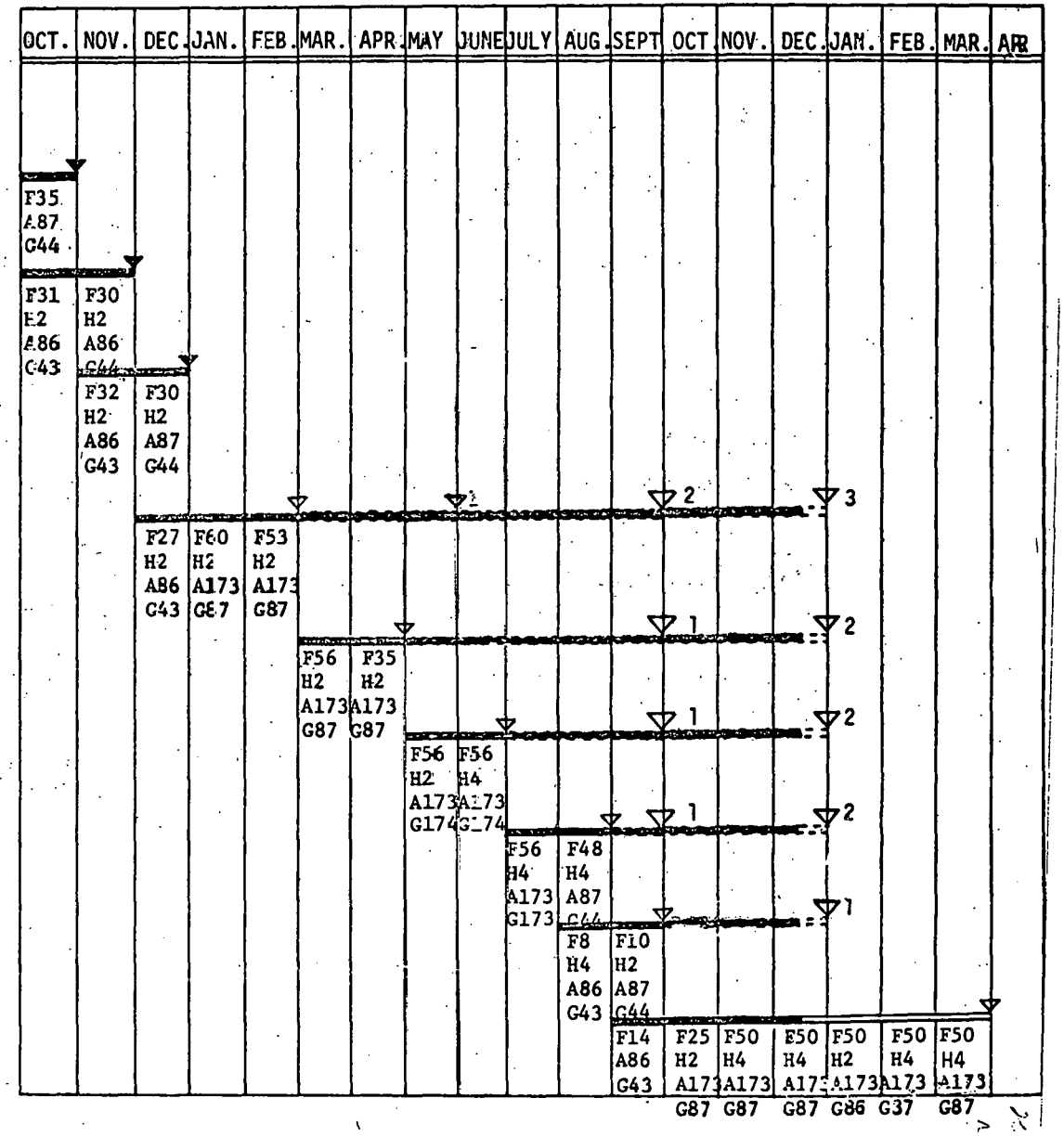

1.3 Web growth analysis

1.3.1 Develop semi-empirical multivariate static model from web growth manual experiments

1.3.2 Thermal web growth analysis

1.3.3 Correlate analysis, experimental data, and semi-empirical model

2. Web Characterization

2.1 Development of sampling strategy, prototype technique

2.2 Structural characterization

2.3 Electrical characterization, web bulk silicon

2.4 Electrical characterization, web solar cells

3. Documentation, Program Review

3.1 Documentation

3.1.1 Initial financial management report and program plan

3.1.2 NASA Form 533M MAR 73, JPL 3645, JPL 3645-1

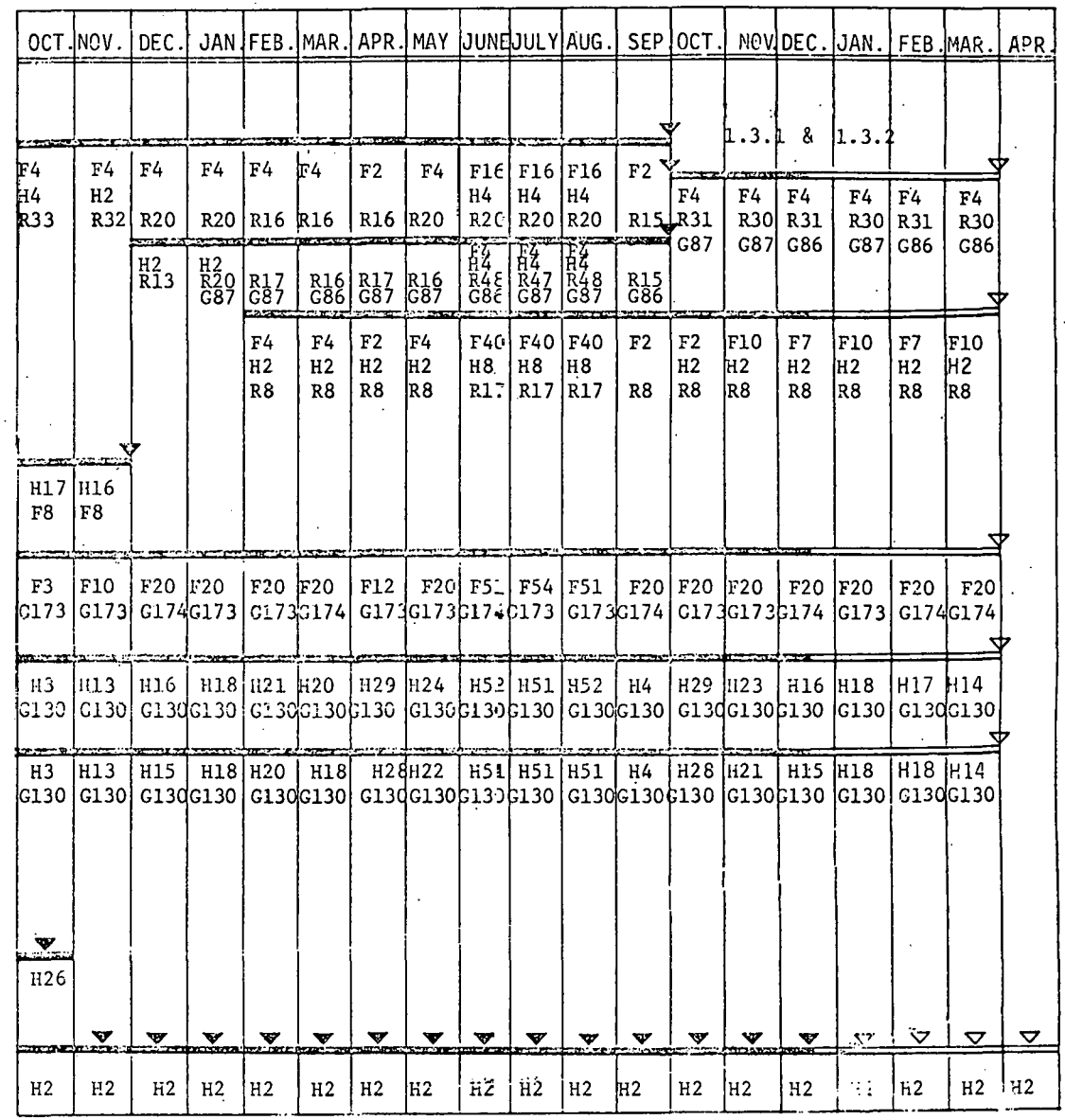

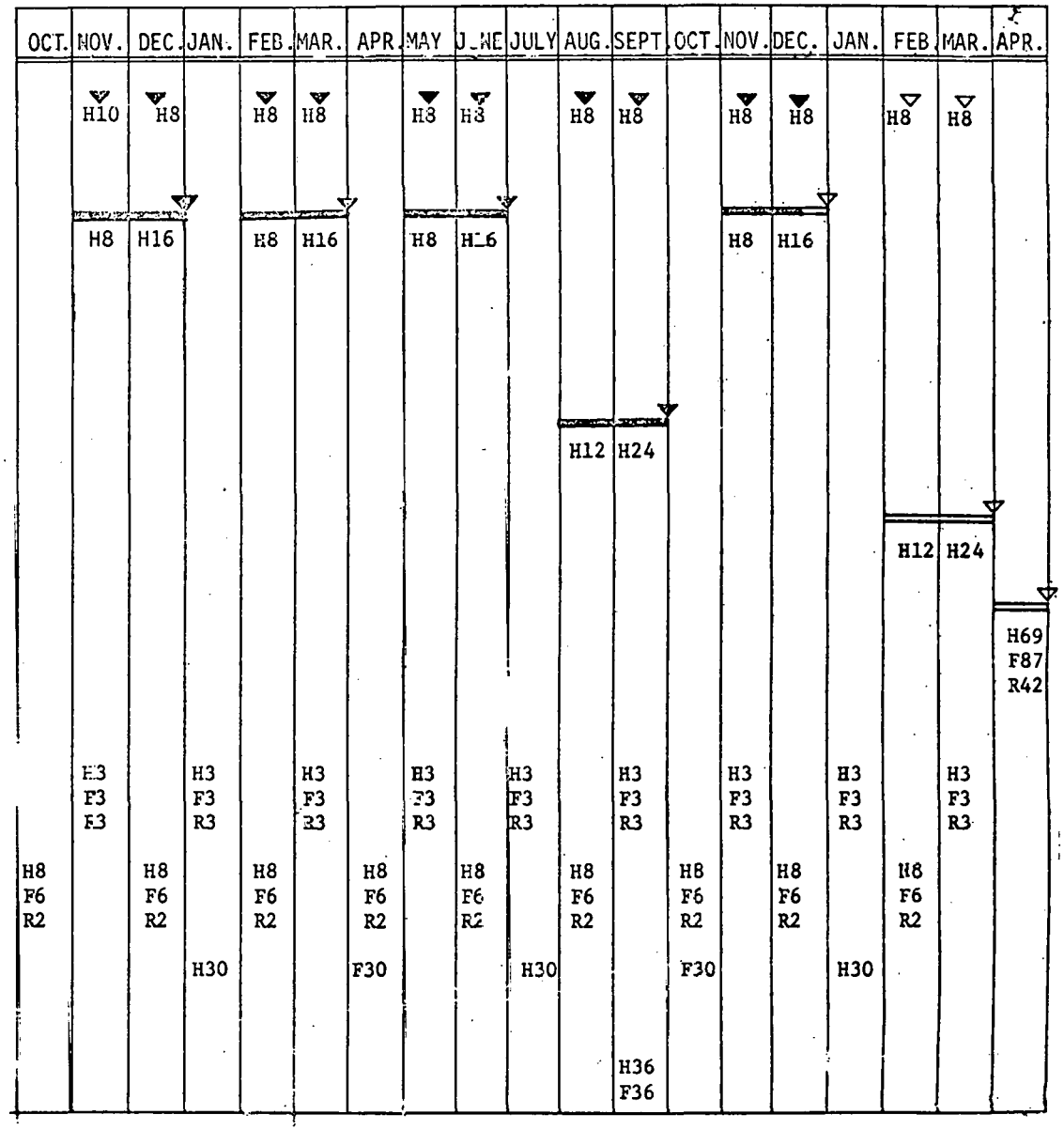
OCT.
NOV.
DEC.
JAN.
FEB.
MAR.
APR.
MAY
JUNE
JULY
AUG.
SEPT.
OCT.
NOV.
DEC.
JAN.
FEB.
MAR.
APR.
3.1.3 Monthly technical progress report
H10 H8 H8 H8 H8 H8 H8 H8 H8 H8 H8 H8
3.1.4 Quarterly report
H8 H16 H8 H16 H8 H16 H8 H16 H8 H16
3.1.5 Interim summary
3.1.6 Annual report
H12 H24
3.1.7 Draft final report
H12 H24
3.1.8 Approved final report
H69
F87
R42
3.2 Program review, work sessions
3.2.1 USC in-house review
H3 F3 R3
3.2.2 JPL program review
H8 F6 R2
3.2.3 Task integration sessions
H30 F30 H30 F30 H30
3.2.4 Annual workshop
H36
F36

	OCT.	NOV	DEC.	JAN.	FEB.	MAR.	APR.	MAY	JUNE	JULY	AUG.	SEP.	OCT.	NOV	DEC.	JAN.	FEB	MAR	APR.
3.2.5 Design and performance review						▽1													
4. General Administration	H22 S87	H16 S87	H16 S87	H12 S87	H16 S87	H16 S87	H16 S87	H16 S87	H15 S87	H16 S87	H16 S87	H4 S87	H16 S87	H16 S87	H16 S87	H12 S87	H16 S87	H16 S87	H16 S87
5. Planned Cost (Thousands of dollars)	12.5	16.8	14.2	14.3	12.7	13.0	13.3	12.6	17.8	19.1	17.2	15.5	13.5	12.8	13.0	13.4	12.8	13.2	7.1
Incurred Cost (Thousands of dollars)																			